



Application of Copper Iodide Nanoparticle-Doped Film and Fabric To Inactivate SARS-CoV-2 via the Virucidal Activity of Cuprous Ions (Cu⁺)

Yohei Takeda,^{a,b} Dulamjav Jamsransuren,^b Tomokazu Nagao,^c Yoko Fukui,^c Sachiko Matsuda,^b  Haruko Ogawa^b

^aResearch Center for Global Agromedicine, Obihiro University of Agriculture and Veterinary Medicine, Obihiro, Hokkaido, Japan

^bDepartment of Veterinary Medicine, Obihiro University of Agriculture and Veterinary Medicine, Obihiro, Hokkaido, Japan

^cEmergent Research Center, R&D Headquarter, NBC Meshtec Inc., Hino, Tokyo, Japan

ABSTRACT As a result of the novel coronavirus disease 2019 pandemic, strengthening control measures against severe acute respiratory syndrome coronavirus 2 (SARS-CoV-2) has become an urgent global issue. In addition to antiviral therapy and vaccination strategies, applying available virucidal substances for SARS-CoV-2 inactivation is also a target of research to prevent the spread of infection. Here, we evaluated the SARS-CoV-2 inactivation activity of a copper iodide (CuI) nanoparticle dispersion, which provides Cu⁺ ions having high virucidal activity, and its mode of actions. In addition, the utility of CuI-doped film and fabric for SARS-CoV-2 inactivation was evaluated. The CuI dispersion exhibited time-dependent rapid virucidal activity. Analyses of the modes of action of CuI performed by Western blotting and real-time reverse transcription-PCR targeting viral proteins and the genome revealed that CuI treatment induced the destruction of these viral components. In this setting, the indirect action of CuI-derived reactive oxygen species contributed to the destruction of viral protein. Moreover, the CuI-doped film and fabric demonstrated rapid inactivation of the SARS-CoV-2 solution in which the viral titer was high. These findings indicated the utility of the CuI-doped film and fabric as anti-SARS-CoV-2 materials for the protection of high-touch environmental surfaces and surgical masks/protective clothes. Throughout this study, we demonstrated the effectiveness of CuI nanoparticles for inactivating SARS-CoV-2 and revealed a part of its virucidal mechanism of action.

IMPORTANCE The COVID-19 pandemic has caused an unprecedented number of infections and deaths. As the spread of the disease is rapid and the risk of infection is severe, hand and environmental hygiene may contribute to suppressing contact transmission of SARS-CoV-2. Here, we evaluated the SARS-CoV-2 inactivation activity of CuI nanoparticles, which provide the Cu⁺ ion as an antiviral agent, and we provided advanced findings of the virucidal mechanisms of action of Cu⁺. Our results showed that the CuI dispersion, as well as CuI-doped film and fabric, rapidly inactivated SARS-CoV-2 with a high viral titer. We also demonstrated the CuI's virucidal mechanisms of action, specifically the destruction of viral proteins and the genome by CuI treatment. Protein destruction largely depended on CuI-derived reactive oxygen species. This study provides novel information about the utility and mechanisms of action of promising virucidal material against SARS-CoV-2.

KEYWORDS antiviral fabric, antiviral film, copper iodide nanoparticle, cuprous ion, SARS-CoV-2

Since the first identification of severe acute respiratory syndrome coronavirus 2 (SARS-CoV-2) in December 2019 (1), this novel virus has spread worldwide rapidly, and the seriousness of the severe impacts of the novel coronavirus disease 19 (COVID-19)

Citation Takeda Y, Jamsransuren D, Nagao T, Fukui Y, Matsuda S, Ogawa H. 2021. Application of copper iodide nanoparticle-doped film and fabric to inactivate SARS-CoV-2 via the virucidal activity of cuprous ions (Cu⁺). *Appl Environ Microbiol* 87:e01824-21. <https://doi.org/10.1128/AEM.01824-21>.

Editor Karyn N. Johnson, University of Queensland

Copyright © 2021 American Society for Microbiology. All Rights Reserved.

Address correspondence to Haruko Ogawa, hogawa@obihiro.ac.jp.

Received 15 September 2021

Accepted 23 September 2021

Accepted manuscript posted online 6 October 2021

Published 24 November 2021

pandemic is still ongoing at the time of this publication (<https://www.who.int/emergencies/diseases/novel-coronavirus-2019/situation-reports>). Under this unprecedented crisis, considerable efforts have been made to overcome the pandemic, and many therapeutic drug candidates and vaccine products have been manufactured at dramatic speed. However, therapeutic knowledge is still insufficient to provide a beneficial effect in all patients, and the rapid emergence of mutant strains is a concern for vaccine efficacy (2). Hence, as another infection prevention measure to supplement therapeutic and vaccination strategies, applying available virucidal substances against SARS-CoV-2 for hand and environmental hygiene is also of interest.

The dominant transmission of SARS-CoV-2 is via inhalable respiratory aerosols, and there is substantial evidence that wearing a mask, ventilation, and keeping a distance are the primary infection prevention measures (<https://www.who.int/news-room/q-a-detail/coronavirus-disease-covid-19-how-is-it-transmitted>; <https://www.cdc.gov/coronavirus/2019-ncov/science/science-briefs/sars-cov-2-transmission.html>). Additionally, direct contact transmission via contaminated hand is also a possible transmission mode. However, indirect transmission via contaminated environmental surfaces is considered a rare transmission mode. Although there seems to be a common view among experts that hand hygiene has a certain effect on preventing direct and indirect contact transmissions, the effectiveness of environmental hygiene has not been clarified (3). Nevertheless, SARS-CoV-2 RNA was detected on many environmental surfaces, especially high-touch surfaces in hospitals (4, 5); infectious viruses were also recovered from environmental surfaces where COVID-19 patients stayed and patients' hands (6). In such a situation, the countermeasure to environmental hygiene cannot be ignored completely, and SARS-CoV-2 infection control guidelines established by many medical sectors describe the implementation of environmental cleaning as well as hand hygiene.

Many experimental studies in the laboratory have assessed the duration of the infectious stability of SARS-CoV-2 on various surfaces. Although the applicability of these studies to real-world conditions has been disputed (7), SARS-CoV-2 maintained infectivity on plastic, stainless steel, cardboard, and glass surfaces for more than 24 h at room temperature in some experimental settings (8–10). The duration of the infectious stability of SARS-CoV-2 lasted several times longer than that of the influenza A virus on polyethylene, stainless steel, and borosilicate glass surfaces (10). In addition, SARS-CoV-2 maintained infectivity for several days on surgical and N95/N100 masks (11, 12). On the other hand, SARS-CoV-2 on a copper surface was inactivated more rapidly than on other materials. The half-life times of 50 μ l SARS-CoV-2 solution, for which the viral titer was 5- \log_{10} 50% tissue culture infective dose (TCID₅₀)/ml, when applied on copper, cardboard, stainless steel, and plastic surfaces, were 0.77, 3.64, 5.63, and 6.81 h, respectively (9). Copper has antibacterial, antifungal, and antiviral activities (13). The virucidal activity of copper against multiple virus species, including the influenza A virus, human immunodeficiency virus, norovirus, and herpes simplex virus, was reported (13–15). There are mainly two types of copper ions: one is a cupric ion (Cu²⁺), and the other is a cuprous ion (Cu⁺). We focused specifically on the strong antimicrobial activities of Cu⁺. Our team's previous research demonstrated that the copper iodide (CuI) nanoparticle-doped nylon mesh inhibited the attachment of sea organisms for more than 249 days (16). Those studies also revealed the virucidal activities of CuI nanoparticle dispersion against the influenza A virus and feline calicivirus, which is surrogate virus of the human norovirus (17, 18). In research targeting the feline calicivirus, CuI nanoparticle dispersion (Cu⁺ ion) showed more potent virucidal activity than CuCl₂·2H₂O solution (Cu²⁺ ion) (18). Another research group also demonstrated the possibility that Cu⁺ is more effective than Cu²⁺ in the inactivation of the murine norovirus on a copper surface (19).

In this study, we investigated the SARS-CoV-2-inactivating activities of CuI nanoparticle dispersion and CuI nanoparticle-doped film and fabric. Additionally, we analyzed the virucidal mechanisms of action of CuI. This study aimed to obtain advanced

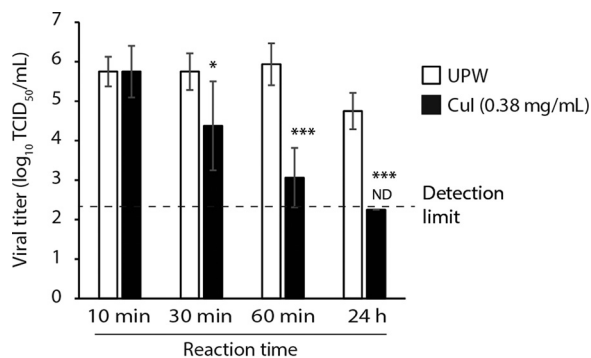


FIG 1 Evaluation of the virucidal activity of the copper iodide (Cul) dispersion. The severe acute respiratory syndrome coronavirus 2 solution was mixed with the Cul dispersion or ultrapure water (UPW). The Cul concentration in the mixture of the Cul group was 0.38 mg/ml. After 10 min to 24 h of reaction time, the viral titer of each test group was measured. Results are indicated as the mean \pm SD ($n = 8$ to 12 per group). Student's t test was performed to analyze the statistical significance between the UPW and Cul groups. *, $P < 0.05$; ***, $P < 0.001$; ND, not detected.

knowledge related to the availability of Cul nanoparticles as an antiviral material, which can contribute to the prevention of spread of SARS-CoV-2 infection.

RESULTS

Evaluation of the virucidal activity of Cul dispersion. The mixtures of SARS-CoV-2 solution and ultrapure water (UPW) or Cul dispersion were agitated by inverting for 10 min to 24 h, and then the viral titers were compared between the UPW and 0.38-mg/ml Cul groups. Although the viral titer of the Cul group was comparable to that of the UPW group at the 10-min reaction time, the viral titer of the Cul group was significantly lower than that of the UPW group at 30 min, 60 min, and 24 h of reaction time. The reduction of the viral titer by Cul treatment, which means the difference in viral titers between the UPW and Cul groups, was ≥ 1.38 -, ≥ 2.88 -, and ≥ 2.50 -log₁₀ TCID₅₀/ml at 30 min, 60 min, and 24 h, respectively; the viral titer was below the detection limit for the Cul group at 24 h (Fig. 1). This result indicated that Cul dispersion shows time-dependent SARS-CoV-2 inactivation activity.

Evaluation of the impact of Cul dispersion on viral structural proteins. The virus was treated with 0.38 mg/ml Cul for 24 h, followed by Western blotting (WB) analyses to detect the S protein S1 subunit, S2 subunit, and N protein. The UPW-treated virus was also analyzed as a control. As a result, there were no differences in the band patterns of the three proteins between the UPW and Cul groups (Fig. 2A). To evaluate the direct impact of Cul treatment on each viral structural protein more specifically, each recombinant protein was treated with UPW or 0.38 mg/ml Cul for 0 h (no reaction time) or 12 h, and then WB analyses were performed. The band patterns of the three proteins were similar between the UPW and Cul groups at 0 h. On the other hand, although the specific bands of the three proteins were detected in the UPW group at 12 h, these bands were not detected in the Cul group (Fig. 2B). Then, the virus was treated with UPW or 3.8 mg/ml Cul for 0 or 24 h, and WB analyses were performed. The band patterns of the three proteins were similar between the UPW and Cul groups at 0 h. On the other hand, the band patterns of the three proteins were different between the UPW and Cul groups at 24 h. Specifically, when the S1 subunit of the WB was detected, the intensities of the ~ 150 - and ~ 250 -kDa bands were weaker in the Cul group than in the UPW group, and another band with a higher molecular mass was detected under Cul treatment (Fig. 2C, left). When the S2 subunit was detected in the WB, the intensities of the ~ 130 - and > 250 -kDa bands were weaker in the Cul group than in the UPW group, and bands representing high-molecular-weight proteins at > 250 kDa were detected under Cul treatment (Fig. 2C, middle). When the N protein was detected in the WB, the specific band disappeared in the Cul group (Fig. 2C, right).

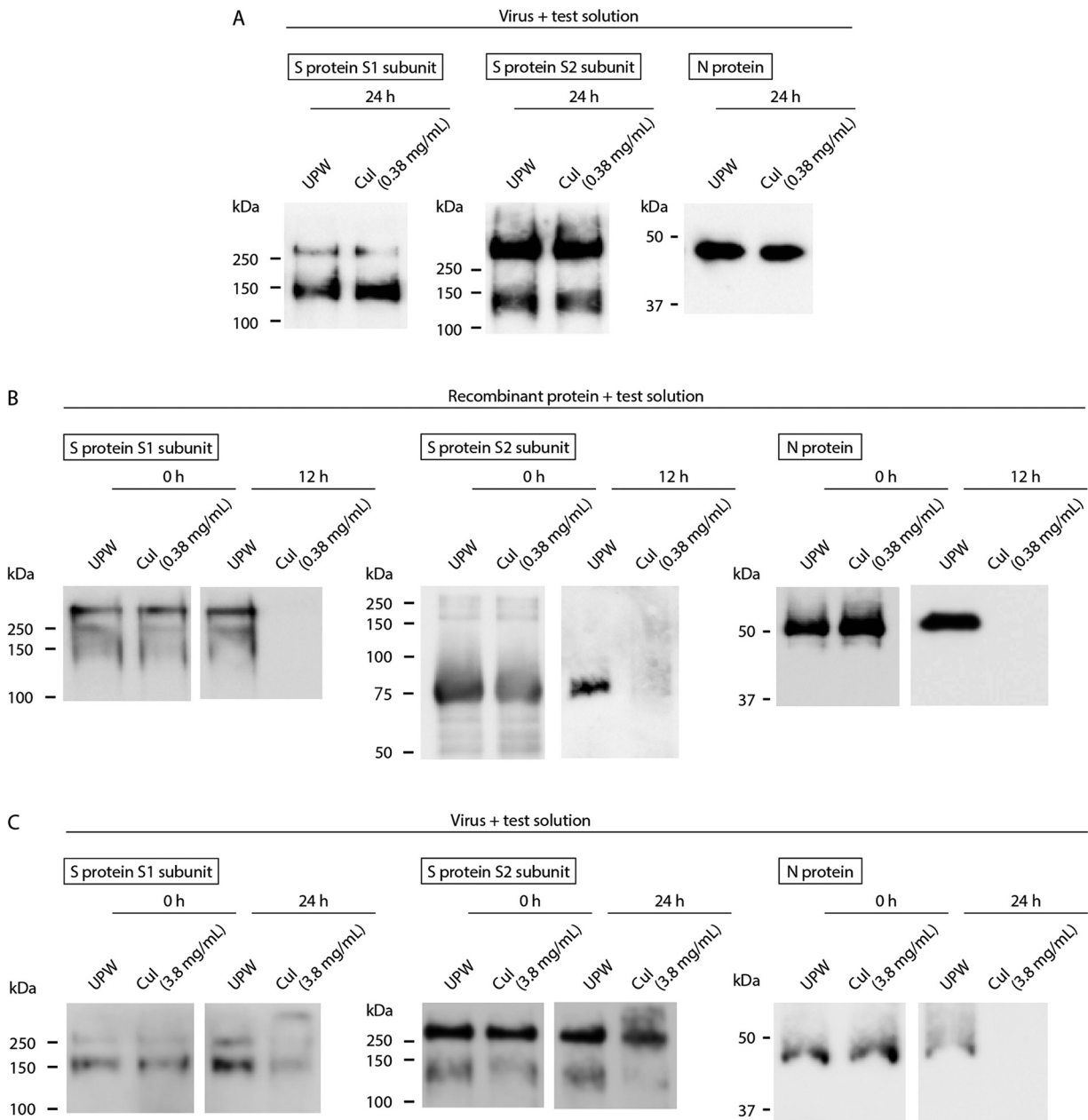


FIG 2 Evaluation of the impact of the copper iodide (Cul) dispersion on viral structural proteins. (A and C) The severe acute respiratory syndrome coronavirus 2 solution was mixed with the Cul dispersion or ultrapure water (UPW). The Cul concentration in the mixture of the Cul group was 0.38 mg/ml (A) or 3.8 mg/ml (C). After 24 h (A) or 0 and 24 h (C) reaction time, Western blotting (WB) analyses to detect the S protein S1 subunit, S2 subunit, and N protein were performed. (B) Recombinant proteins were mixed with the Cul dispersion or UPW. The Cul concentration in the mixture of the Cul group was 0.38 mg/ml. After 0 and 12 h reaction time, WB analyses were performed.

Evaluation of the impact of the Cul-derived reactive oxygen species on viral structural protein.

Our previous reports showed that reactive oxygen species (ROS) are generated from Cul dispersion (17, 18). To evaluate the contribution of Cul-derived ROS to Cul-induced structural change in or destruction of the viral protein, the recombinant protein was treated with 0.38 mg/ml Cul for the indicated reaction times in the presence or absence of *N*-acetyl-L-cysteine (NAC), which is an ROS scavenger, followed by WB analyses. Here, recombinant S protein S2 subunit was analyzed as a representative protein. In this setting, most parts of hydroxyl radical were considered to be scavenged in the presence of NAC (Fig. S1 in the supplemental material). In either the absence or presence of NAC conditions, there were no differences in the protein

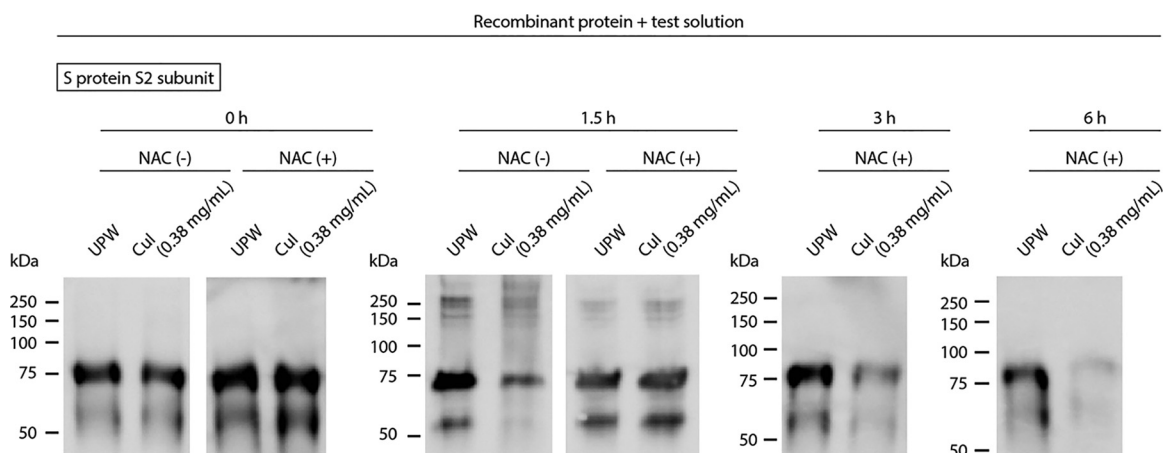


FIG 3 Evaluation of the impact of the copper iodide (Cul)-derived reactive oxygen species on viral structural protein. The recombinant S protein S2 subunit was mixed with the Cul dispersion or ultrapure water (UPW) in the presence or absence of 1.2 mg/ml *N*-acetyl-L-cysteine (NAC). Cul concentration in the mixture of the Cul group was 0.38 mg/ml. After 0, 1.5, 3, and 6 h reaction time, Western blotting analyses to detect the S protein S2 subunit were performed. NAC (–) or NAC (+) indicates the absence or presence of NAC treatment, respectively.

band patterns between the UPW and Cul groups at 0 h. However, the intensities of the bands were weaker in the Cul group than in the UPW group, with an increase in bands representing proteins with molecular weight greater than 75 kDa under Cul treatment in the absence of NAC at 1.5 h. In contrast, there were no differences in the band patterns between those two groups in the presence of NAC at that reaction time. Meanwhile, the intensities of the bands were weaker in the Cul group than in the UPW group in the presence of NAC at 3 and 6 h (Fig. 3).

Evaluation of the impact of Cul dispersion on the viral genome. The virus was treated with 0.38 or 3.8 mg/ml Cul for 0 or 24 h, followed by real-time reverse transcription-PCR (RT-PCR) targeting the viral genome. The UPW-treated virus was also analyzed as a control. The cycle threshold (C_T) value for the 0.38-mg/ml Cul treatment was comparable to that of the UPW group at 0 h. On the other hand, the C_T value of the Cul group was statistically higher than that of the UPW group at 24 h; the difference in the C_T values between the UPW and Cul groups was 1.47 (Fig. 4A). Then, the virus treated with 3.8 mg/ml Cul was analyzed. The C_T value of the Cul group was slightly higher than that of the UPW group at 0 h; the difference in the C_T values between the UPW and Cul groups was 0.75. In addition, the C_T value of the Cul group was clearly higher than that of the UPW group at 24 h; the difference in the C_T values between the UPW and Cul groups was 10.37 (Fig. 4B).

Evaluation of the virucidal activities of Cul-doped film and fabric. The SARS-CoV-2 solution was covered by nondoped or Cul-doped film and incubated for each reaction time; then, the viral titers were compared between the nondoped and Cul-doped film groups. The viral titer in the Cul-doped film group was comparable to that in the nondoped film group at 1 min, while those in the Cul-doped film group were significantly lower than that of the nondoped film group at 10, 60, and 120 min. The reduction of the viral titer by the Cul-doped film was 0.75-, ≥ 1.94 -, and ≥ 2.69 -log₁₀ TCID₅₀/ml at 10, 60, and 120 min, respectively (Fig. 5A). The virucidal activity of the Cul-doped fabric was also evaluated. The viral titer in the Cul-doped fabric group was comparable to that in the nondoped fabric group at 1 min, while those of the Cul-doped fabric group were significantly lower than that of the nondoped fabric group at 30 and 60 min. The reduction of the viral titer by the Cul-doped fabric was 0.59- and ≥ 1.63 -log₁₀ TCID₅₀/ml at 30 and 60 min, respectively. Although the viral titer of the Cul-doped fabric group was below the detection limit at 120 min, that of the nondoped fabric group was similarly low, and there was no significant difference between these two groups (Fig. 5B).

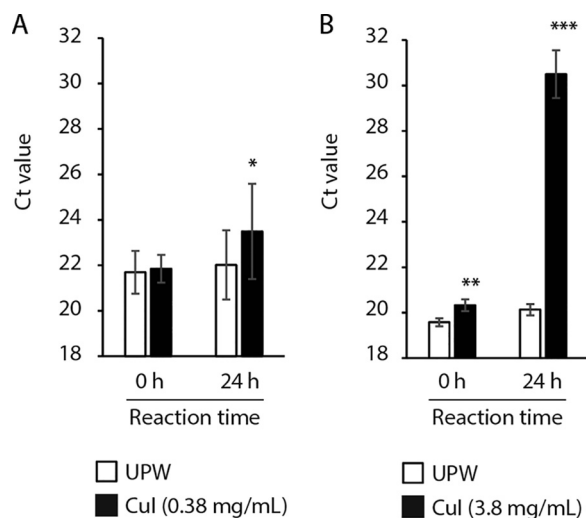


FIG 4 Evaluation of the impact of the copper iodide (CuI) dispersion on the viral genome. (A and B) Severe acute respiratory syndrome coronavirus 2 (SARS-CoV-2) solution was mixed with the CuI dispersion or ultrapure water (UPW). The CuI concentration in the mixture of the CuI group was 0.38 mg/ml (A) or 3.8 mg/ml (B). After 0 and 24 h reaction time, real-time reverse transcription-PCR targeting the N gene of SARS-CoV-2 was performed, and the cycle threshold (C_t) value was calculated. Results are indicated as the mean \pm SD ($n = 4$ per group). Student's t test was performed to analyze the statistical significance between the UPW and CuI groups. *, $P < 0.05$; **, $P < 0.01$; ***, $P < 0.001$.

DISCUSSION

Here, we reported the time-dependent virucidal activity of CuI nanoparticles against SARS-CoV-2 in liquid, film, and fabric. It has been reported that the speed of SARS-CoV-2 inactivation is proportional to the increase in temperature and relative humidity (20). The conditions of temperature and relative humidity in the present study were 22°C to 25°C and 45% to 50% relative humidity, which reflected the common indoor environments and were relatively close to the conditions in the previous studies (20°C to 25°C, 35% to 65% relative humidity), which evaluated the stability of SARS-CoV-2 on the surfaces (8–10, 12).

One of the important factors contributing to the antimicrobial activity of copper is the generation of ROS from copper ions (13). Cu^+ , as well as Cu^{2+} , generates a hydroxyl radical in the presence of H_2O_2 by a Fenton-like reaction (21). In addition, Cu^+ gener-

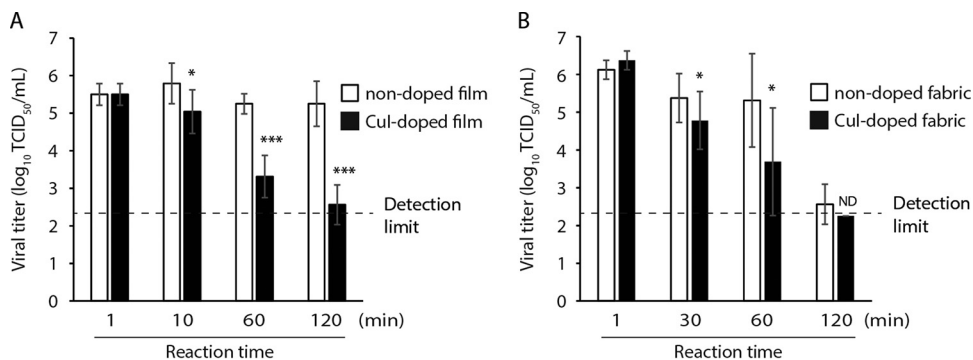


FIG 5 Evaluation of the virucidal activities of copper iodide (CuI)-doped film and fabric. (A) Severe acute respiratory syndrome coronavirus 2 (SARS-CoV-2) solution was covered with CuI-doped and nondoped films. After 1 to 120 min reaction time, the viral titer of each test group was measured. (B) SARS-CoV-2 solution was soaked into CuI-doped and nondoped fabrics. After 1 to 120 min reaction time, the viral titer of each test group was measured. Results are indicated as the mean \pm SD ($n = 4$ to 16 per group). Student's t test was performed to analyze the statistical significance between the nondoped and CuI-doped groups. *, $P < 0.05$; ***, $P < 0.001$; ND, not detected.

ates a hydroxyl radical even in the absence of H_2O_2 , such as under a cell-free condition (16–18). Our team's previous study showed that the CuI suspension, but not the $\text{CuSO}_4 \cdot 5\text{H}_2\text{O}$ solution, generated a hydroxyl radical (17). Our previous study also suggested that the more potent virucidal activity of Cu^+ than that of Cu^{2+} against the feline calicivirus was partially due to the presence of hydroxyl radical generation (18). In contrast, another study against the murine norovirus suggested that the virucidal activity of the copper surface did not rely on hydroxyl radicals and superoxide (19). The result of Fig. 3 at 1.5 h reaction time showed that CuI-derived ROS largely contributed to structural change in or destruction of the viral protein. Moreover, although it is difficult to completely deny the contribution of small amounts of residual ROS, which were not scavenged by NAC, the result of Fig. 3 at 3 h and 6 h suggests the impact of ROS-independent action. These findings indicate that virus inactivation by Cu^+ results from direct and indirect Cu^+ activity via the production of ROS.

In the present study, WB analyses did not show any abnormalities of the band patterns of S proteins and N proteins in the virus particles treated with 0.38 mg/ml CuI at 24 h (Fig. 2A). On the other hand, the band patterns and intensities changed dramatically when the recombinant virus proteins or virus particles were treated with 0.38 mg/ml CuI at 12 h or 3.8 mg/ml CuI at 24 h, respectively (Fig. 2B and C). These results indicated that there was a more significant impact of CuI on recombinant proteins than on proteins in viral particles. Such a discrepancy in recombinant proteins and viral particles was also observed in our previous study using a polyphenol-rich virucidal natural component (22). As S proteins are expressed in close proximity and N proteins are located inside the viral particles, the restriction of physical contact of Cu^+ to these proteins may have lowered its impact on proteins in the viral particles. In another possibility, the difference in the level of organic load in the recombinant protein solution (fetal bovine serum free) and the SARS-CoV-2 solution (containing 1% fetal bovine serum) may have influenced the discrepancy of the results. To evaluate the impact of organic load on CuI nanoparticle-dependent virucidal activity, the analysis targeting purified SARS-CoV-2 should be performed in future studies. Notably, such an impact of CuI on viral proteins was observed against the influenza A virus (17). Our findings indicate that CuI induces structural changes in or destruction of the virus protein concentration dependently; 0.38 mg/ml CuI might have induced small abnormalities in the proteins in SARS-CoV-2 particles, even though such abnormalities were not detected by WB. The previous study revealed that some amino acids on the viral capsid protein of the feline calicivirus were oxidized by CuI treatment (18). As ROS induce protein damage (23), such oxidative damage might have impacted the function of SARS-CoV-2 proteins.

Another plausible SARS-CoV-2-inactivating mechanism of CuI is the destruction of the viral envelope. Cu^+ and Cu^{2+} induce lipid peroxidation (24), which results in biological membrane damage. Santo et al. (25) demonstrated that copper-induced membrane damage on bacteria may have contributed to bactericidal activity. Although electron microscopic observations of the envelope structure of CuI-treated SARS-CoV-2 particles was beyond the scope of the current study because of the safe handling of pathogens, rapid SARS-CoV-2 inactivation by CuI may have been caused by the destruction of the viral envelope.

This study also suggested that the viral genome was disrupted by CuI treatment (Fig. 4). Although the increase in C_T value by 0.38 mg/ml CuI treatment was limited, it should be taken into account that the low C_T value does not directly suggest the large amounts of the intact whole viral genome and infectious viral particles. Even though the increase of C_T value was limited, the 0.38 mg/ml CuI might have impacted not only the specific target region analyzed by current real-time RT-PCR but also other multiple parts of the viral genome. Nevertheless, many residual viral RNA signals at low CuI concentrations may be due to the consumption of CuI by the interaction with viral proteins, envelope, and organic substances contained in the viral solution. The mode of action of CuI on the viral genome was consistent with a previous report that suggested that Cu^+ -derived ROS induced nucleic acid damage (26). Although it was unclear

whether the impacts of CuI on viral proteins and the genome were critical for rapid virus inactivation, these modes of action would be involved in the overall process of SARS-CoV-2 inactivation by CuI.

In this study, ~ 5.1 - and ~ 5.8 -log₁₀ TCID₅₀/60 μ l were applied to 2.25 cm² of CuI-doped film and fabric, respectively, and virucidal activities were observed within 30 min (Fig. 5). These viral loads are considered to be much higher than those found on actual contaminated environmental surfaces (6, 27). Although the influences of the coexisting organic substances contained in saliva and mucous with the virus were not assessed in this study, the duration of the infectious stability of SARS-CoV-2 on surfaces tended to be shorter in the presence of mucus and sputum, which contain antiviral components (10, 28). Therefore, CuI-doped film and fabric are assumed to be capable of exerting virucidal activity sufficiently in real-world environments. Behzadinasab et al. (29) reported that the surface coating of Cu₂O particles bound with polyurethane demonstrated SARS-CoV-2 inactivation within 1 h. As with Cu₂O coatings, CuI-doped film and CuI coatings can be applied to high-touch surfaces. Meanwhile, CuI-doped fabric can be used in surgical masks, protective clothing, and antiviral cloths. CuI nanoparticles have been proven to achieve high safety through acute oral toxicity tests (50% lethal dose [LD₅₀], >2,000 mg/kg), eye irritation tests, primary skin irritation tests, skin sensitization tests (no irritating reactions), and mutagenicity tests (internal data in NBC Meshtec, Inc., Tokyo, Japan). Hence, it can be applied to not only environmental surfaces but also hand hygiene. In this study, we demonstrated the potential of CuI nanoparticles as a promising anti-SARS-CoV-2 material and revealed a part of its virucidal mechanism of action, which can contribute to strengthening SARS-CoV-2 control measures.

MATERIALS AND METHODS

Test samples. The powders of CuI nanoparticles (Cufitec) and CuI nanoparticle-doped film and fabric (Cufitec-doped polyethylene terephthalate film and rayon nonwoven fabric) were provided by NBC Meshtec Inc. The CuI dispersion was prepared by adding the CuI powder to UPW. The UPW was used as a solvent control. The CuI content in the CuI-doped film remains confidential. The CuI content in the CuI-doped fabric was 0.5 wt%. Polyethylene terephthalate film and rayon nonwoven fabric without CuI were used as base controls for the CuI-doped film and fabric, respectively.

Virus and cells. The 2019-nCoV/Japan/TY/WK-521/2020 strain of SARS-CoV-2 was kindly provided by the National Institute of Infectious Diseases (Tokyo, Japan). Samples of the VeroE6/TMPRSS2 cell (30), which was established by the National Institute of Infectious Diseases, were obtained from the Japanese Collection of Research Bioresources (Osaka, Japan; cell no. JCRB1819). SARS-CoV-2-inoculated VeroE6/TMPRSS2 cells were cultured in the virus growth medium (VGM), which was Dulbecco's modified Eagle's medium (Nissui Pharmaceutical Co., Ltd., Tokyo, Japan) containing 1% fetal bovine serum, 2 mM L-glutamine (Fujifilm Wako Pure Chemical Co., Ltd., Osaka, Japan), 100 μ g/ml kanamycin (Meiji Seika Pharma Co., Ltd., Tokyo, Japan), and 2 μ g/ml amphotericin B (Bristol-Myers Squibb Co., New York, NY, USA).

Evaluation of virucidal activity of CuI dispersion. The SARS-CoV-2-containing VGM (viral titer, ~ 7.0 -log₁₀ TCID₅₀/ml) was mixed with an equal volume of CuI dispersion. The CuI concentration in the mixture was 0.38 mg/ml. As a control, the SARS-CoV-2-containing VGM was mixed with an equal volume of UPW. These mixtures were agitated using a rotator for 10 min to 24 h at 22°C to 25°C and 45% to 50% relative humidity; then, nine times the volume of soybean-casein digest broth with lecithin and polysorbate 80 (SCDLP) medium (Nihon Pharmaceutical Co., Ltd., Tokyo, Japan) was added to stop the reaction. Mixtures diluted by SCDLP medium were inoculated into VeroE6/TMPRSS2 cells, and 10-fold serial dilution was performed. After 1 h of incubation at 37°C, the cell culture medium was removed, and a new VGM was added. After 3 days of incubation at 37°C, a cytopathic effect on the cells was observed, and the viral titer (log₁₀ TCID₅₀/ml) was calculated by the Behrens-Kärber method (31).

WB analysis. WB was performed as we described previously (22). Briefly, the SARS-CoV-2-containing VGM or 40 μ g/ml of the recombinant protein (SARS-CoV-2 S protein S1 subunit, S protein S2 subunit, or N protein) was mixed with an equal volume of the CuI dispersion or UPW. The CuI concentrations in the mixture were 0.38 and 3.8 mg/ml or 0 mg/ml (UPW group). At that time, 1.2 mg/ml NAC (Fujifilm Wako Pure Chemical Co.) was added to some mixtures to scavenge ROS. These mixtures were combined with sodium dodecyl sulfate (SDS) buffer with 2-mercaptoethanol (Fujifilm Wako Pure Chemical Co.) either immediately (0 h reaction time) or were agitated for 1.5, 3, 6, 12, or 24 h at 22°C to 25°C and 45% to 50% relative humidity prior to adding the SDS buffer (1.5, 3, 6, 12, or 24 h reaction time). The mixed samples were subjected to WB analyses.

Real-time RT-PCR analyses. The SARS-CoV-2-containing VGM was mixed with an equal volume of the CuI dispersion or UPW. The CuI concentrations in the mixture were 0.38 and 3.8 mg/ml or 0 mg/ml (UPW group). These mixtures were combined with Isogen-LS (Nippon Gene Co., Ltd., Tokyo, Japan) immediately (0 h reaction time), or were agitated for 24 h at 22°C to 25°C and 45% to 50% relative humidity prior to the addition of Isogen-LS (24 h reaction time). The samples were subjected to real-time RT-PCR

analysis, as described previously (22). The primers and probe used in this study were NIID_2019-nCoV_N_F2, NIID_2019-nCoV_N_R2, and NIID_2019-nCoV_N_P2, which targeted the region of the N gene of SARS-CoV-2 (32).

Evaluation of virucidal activity of Cul-doped film. A volume of 60 μ l of SARS-CoV-2 solution (viral titer, $\sim 5.1\text{-log}_{10}$ TCID₅₀/60 μ l) was placed on the turned-over lid of a 12-well plate (Nunc, Rochester, NY, USA). This virus solution was covered with 2.25 cm² (1.5 cm by 1.5 cm) of Cul-doped film or nondoped film, and the film was placed at 22°C to 25°C and 45% to 50% relative humidity for 1 to 120 min. Then, the virus was collected using nine times the volume of SCDLP medium. This virus recovery solution was inoculated into the cells, and 10-fold serial dilution was performed. The medium was changed after 1 h of incubation at 37°C, and the viral titer was calculated as mentioned above.

Evaluation of the virucidal activity of Cul-doped fabric. The 2.25 cm² (1.5 cm by 1.5 cm) Cul-doped fabric or nondoped fabric was placed on the 12-well plate, and 60 μ l of SARS-CoV-2 solution (viral titer, $\sim 5.8\text{-log}_{10}$ TCID₅₀/60 μ l) was soaked into the fabric. The fabric was placed at 22°C to 25°C and 45% to 50% relative humidity for 1 to 120 min, and then nine times the volume of SCDLP medium was soaked into the fabric. The fabric and SCDLP medium were collected into a screw cap tube (Scientific Specialties Inc., Lodi, CA, USA), and the tube was vortexed. This virus recovery solution was inoculated into the cells, and 10-fold serial dilution was performed. The medium was changed after 1 h of incubation at 37°C, and the viral titer was calculated as mentioned above.

Statistical analyses. The statistical significance of the difference in viral titer between the control group and each Cul group was analyzed using Student's *t* test. *P* values of less than 0.05 were considered statistically significant.

SUPPLEMENTAL MATERIAL

Supplemental material is available online only.

SUPPLEMENTAL FILE 1, PDF file, 0.2 MB.

ACKNOWLEDGMENTS

We thank Enago for English language editing.

We declare no conflicts of interest. This research did not receive any specific grant from funding agencies in the public, commercial, or not-for-profit sectors.

REFERENCES

- Zhu N, Zhang D, Wang W, Li X, Yang B, Song J, Zhao X, Huang B, Shi W, Lu R, Niu P, Zhan F, Ma X, Wang D, Xu W, Wu G, Gao GF, Tan W, China Novel Coronavirus Investigating and Research Team. 2020. A novel coronavirus from patients with pneumonia in China, 2019. *N Engl J Med* 382:727–733. <https://doi.org/10.1056/NEJMoa2001017>.
- Collier DA, De Marco A, Ferreira IATM, Meng B, Dattir R, Walls AC, Kemp SS, Bassi J, Pinto D, Fregni CS, Bianchi S, Tortorici MA, Bowen J, Culap K, Jacconi S, Cameron E, Snell G, Pizzuto MS, Pellanda AF, Garzoni C, Riva A, Elmer A, Kingston N, Graves B, McCoy LE, Smith KGC, Bradley JR, Temperton N, Ceron-Gutierrez L, Barcenas-Morales G, Harvey W, Virgin HW, Lanzavecchia A, Piccoli L, Doffinger R, Wills M, Veessler D, Corti D, Gupta RK, The CITIID-NIHR BioResource COVID-19 Collaboration. 2021. Sensitivity of SARS-CoV-2 B.1.1.7 to mRNA vaccine-elicited antibodies. *Nature* 593:136–141. <https://doi.org/10.1038/s41586-021-03412-7>.
- Dyani L. 2021. COVID-19 rarely spreads through surfaces. So why are we still deep cleaning? *Nature* 590:26–28. <https://doi.org/10.1038/d41586-021-00251-4>.
- Meyerowitz EA, Richterman A, Gandhi RT, Sax PE. 2021. Transmission of SARS-CoV-2: a review of viral, host, and environmental factors. *Ann Intern Med* 174:69–79. <https://doi.org/10.7326/M20-5008>.
- Choi H, Chatterjee P, Coppin JD, Martel JA, Hwang M, Jinadatha C, Sharma VK. 2021. Current understanding of the surface contamination and contact transmission of SARS-CoV-2 in healthcare settings. *Environ Chem Lett* 19:1935–1944. <https://doi.org/10.1007/s10311-021-01186-y>.
- Lin Y-C, Malott RJ, Ward L, Kiplagat L, Pabbaraju K, Gill K, Berenger BM, Hu J, Fonseca K, Noyce R, Louie T, Evans DH, Conly JM. 2021. Detection and quantification of infectious severe acute respiratory coronavirus-2 in diverse clinical and environmental samples from infected patients: evidence to support respiratory droplet, and direct and indirect contact as significant modes of transmission. medRxiv <https://doi.org/10.1101/2021.07.08.21259744>.
- Goldman E. 2020. Exaggerated risk of transmission of COVID-19 by fomites. *Lancet Infect Dis* 20:892–893. [https://doi.org/10.1016/S1473-3099\(20\)30561-2](https://doi.org/10.1016/S1473-3099(20)30561-2).
- Chin AWH, Chu JTS, Perera MRA, Hui KPY, Yen H-L, Chan MCV, Peiris M, Poon LLM. 2020. Stability of SARS-CoV-2 in different environmental conditions. *Lancet Microbe* 1:e10. [https://doi.org/10.1016/S2666-5247\(20\)30003-3](https://doi.org/10.1016/S2666-5247(20)30003-3).
- Doremalen NV, Bushmaker T, Morris DH, Holbrook MG, Gamble M, Williamson BN, Tamin A, Harcourt JL, Thornburg NJ, Gerber SI, Lloyd-Smith JO, Wit ED, Munster VJ. 2020. Aerosol and surface stability of SARS-CoV-2 as compared with SARS-CoV-1. *N Engl J Med* 382:1564–1567. <https://doi.org/10.1056/NEJMc2004973>.
- Hirose R, Ikegaya H, Naito Y, Watanabe N, Yoshida T, Bandou R, Daidoji T, Itoh Y, Nakaya T. 2020. Survival of severe acute respiratory syndrome coronavirus 2 (SARS-CoV-2) and influenza virus on human skin: importance of hand hygiene in coronavirus disease 2019 (COVID-19). *Clin Infect Dis* <https://doi.org/10.1093/cid/ciaa1517>.
- Liu Y, Li T, Deng Y, Liu S, Zhang D, Li H, Wang X, Jia L, Han J, Bei Z, Li L, Li J. 2021. Stability of SARS-CoV-2 on environmental surfaces and in human excreta. *J Hosp Infect* 107:105–107. <https://doi.org/10.1016/j.jhin.2020.10.021>.
- Kasloff SB, Leung A, Strong JE, Funk D, Cutts T. 2021. Stability of SARS-CoV-2 on critical personal protective equipment. *Sci Rep* 11:1–7. <https://doi.org/10.1038/s41598-020-80098-3>.
- Vincent M, Duval RE, Hartemann P, Engels-Deutsch M. 2018. Contact killing and antimicrobial properties of copper. *J Appl Microbiol* 124:1032–1046. <https://doi.org/10.1111/jam.13681>.
- Imai K, Ogawa H, Bui VN, Inoue H, Fukuda J, Ohba M, Yamamoto Y, Nakamura K. 2012. Inactivation of high and low pathogenic avian influenza virus H5 subtypes by copper ions incorporated in zeolite-textile materials. *Antiviral Res* 93:225–233. <https://doi.org/10.1016/j.antiviral.2011.11.017>.
- Sagripanti JL, Routson LB, Bonifacio AC, Lytle CD. 1997. Mechanism of copper-mediated inactivation of herpes simplex virus. *Antimicrob Agents Chemother* 41:812–817. <https://doi.org/10.1128/AAC.41.4.812>.
- Sato T, Fujimori Y, Nakayama T, Gotoh Y, Sunaga Y, Nemoto M, Matsunaga T, Tanaka T. 2012. Assessment of the anti-biofouling potentials of a copper iodide-doped nylon mesh. *Appl Microbiol Biotechnol* 95:1043–1050. <https://doi.org/10.1007/s00253-011-3720-6>.
- Fujimori Y, Sato T, Hayata T, Nagao T, Nakayama M, Nakayama T, Sugamat R, Suzuki K. 2012. Novel antiviral characteristics of nanosized copper(I) iodide particles showing inactivation activity against 2009 pandemic H1N1 influenza virus. *Appl Environ Microbiol* 78:951–955. <https://doi.org/10.1128/AEM.06284-11>.

18. Shionoiri N, Sato T, Fujimori Y, Nakayama T, Nemoto M, Matsunaga T, Tanaka T. 2012. Investigation of the antiviral properties of copper iodide nanoparticles against feline calicivirus. *J Biosci Bioeng* 113:580–586. <https://doi.org/10.1016/j.jbiosc.2011.12.006>.
19. Warnes SL, Keevil CW. 2013. Inactivation of norovirus on dry copper alloy surfaces. *PLoS One* 8:e75017. <https://doi.org/10.1371/journal.pone.0075017>.
20. Biryukov J, Boydston JA, Dunning RA, Yeager JJ, Wood S, Reese AL, Ferris A, Miller D, Weaver W, Zeitouni NE, Phillips A, Freeburger D, Hooper I, Ratnesar-Shumate S, Yolitz J, Krause M, Williams G, Dawson DG, Herzog A, Dabisch P, Wahl V, Hevey MC, Altamura LA. 2020. Increasing temperature and relative humidity accelerates inactivation of SARS-CoV-2 on surfaces. *mSphere* 5:e00441-20. <https://doi.org/10.1128/mSphere.00441-20>.
21. Masarwa M, Cohen H, Meyerstein D, Hickman DL, Bakac A, Espenson JH. 1988. Reactions of low-valent transition-metal complexes with hydrogen peroxide. Are they “Fenton-like” or not? 1. The case of Cu⁺aq and Cr²⁺aq. *J Am Chem Soc* 110:4293–4297. <https://doi.org/10.1021/ja00221a031>.
22. Takeda Y, Jamsransuren D, Matsuda S, Crea R, Ogawa H. 2021. The SARS-CoV-2-inactivating activity of hydroxytyrosol-rich aqueous olive pulp extract (HIDROX) and its use as a virucidal cream for topical application. *Viruses* 13:232. <https://doi.org/10.3390/v13020232>.
23. Stadtman ER, Levine RL. 2003. Free radical-mediated oxidation of free amino acids and amino acid residues in proteins. *Amino Acids* 25:207–218. <https://doi.org/10.1007/s00726-003-0011-2>.
24. Burkitt MJ. 2001. A critical overview of the chemistry of copper-dependent low density lipoprotein oxidation: roles of lipid hydroperoxides, α -tocopherol, thiols, and ceruloplasmin. *Arch Biochem Biophys* 394:117–135. <https://doi.org/10.1006/abbi.2001.2509>.
25. Santo CE, Quaranta D, Grass G. 2012. Antimicrobial metallic copper surfaces kill *Staphylococcus haemolyticus* via membrane damage. *Microbiolopen* 1:46–52. <https://doi.org/10.1002/mbo3.2>.
26. Oikawa S, Kawanishi S. 1998. Distinct mechanisms of site-specific DNA damage induced by endogenous reductants in the presence of iron(III) and copper(II). *Biochim Biophys Acta - Gene Struct Expr* 1399:19–30. [https://doi.org/10.1016/S0167-4781\(98\)00092-X](https://doi.org/10.1016/S0167-4781(98)00092-X).
27. Cheng VC-C, Wong S-C, Chan VW-M, So SY-C, Chen JH-K, Yip CC-Y, Chan K-H, Chu H, Chung TW-H, Sridhar S, To KK-W, Chan JF-W, Hung IF-N, Ho P-L, Yuen K-Y. 2020. Air and environmental sampling for SARS-CoV-2 around hospitalized patients with coronavirus disease 2019 (COVID-19). *Infect Control Hosp Epidemiol* 41:1258–1265. <https://doi.org/10.1017/ice.2020.282>.
28. Bueckert M, Gupta R, Gupta A, Garg M, Mazumder A. 2020. Infectivity of SARS-CoV-2 and other coronaviruses on dry surfaces: potential for indirect transmission. *Materials* 13:5211–5216. <https://doi.org/10.3390/ma13225211>.
29. Behzadinasab S, Chin A, Hosseini M, Poon L, Ducker WA. 2020. A surface coating that rapidly inactivates SARS-CoV-2. *ACS Appl Mater Interfaces* 12:34723–34727. <https://doi.org/10.1021/acsami.0c11425>.
30. Nao N, Sato K, Yamagishi J, Tahara M, Nakatsu Y, Seki F, Katoh H, Ohnuma A, Shirogane Y, Hayashi M, Suzuki T, Kikuta H, Nishimura H, Takeda M. 2019. Consensus and variations in cell line specificity among human metapneumovirus strains. *PLoS One* 14:e0215822. <https://doi.org/10.1371/journal.pone.0215822>.
31. Kärber G. 1931. Beitrag zur kollektiven behandlung pharmakologischer reihenversuche. *Archiv f Experiment Pathol u Pharmakol* 162:480–483. <https://doi.org/10.1007/BF01863914>.
32. Shirato K, Nao N, Katano H, Takayama I, Saito S, Kato F, Katoh H, Sakata M, Nakatsu Y, Mori Y, Kageyama T, Matsuyama S, Takeda M. 2020. Development of genetic diagnostic methods for detection for novel coronavirus 2019(nCoV-2019) in Japan. *Jpn J Infect Dis* 73:304–307. <https://doi.org/10.7883/yoken.JIID.2020.061>.